GNSS Ambiguity-Resolved Detector Implementation With a Lookup Table

Yin, Chengyu; Teunissen, Peter J.G.; Tiberius, Christian C.J.M.

DOI
10.1109/TAES.2025.3632272

Publication date
2026

Document Version
Final published version

Published in
IEEE Transactions on Aerospace and Electronic Systems

GNSS Ambiguity-Resolved Detector: Implementation With a Lookup Table

CHENGYU YIN
Delft University of Technology, Delft, The Netherlands

PETER J.G. TEUNISSEN
Delft University of Technology, Delft, The Netherlands
Curtin University, Perth, Australia

CHRISTIAN C.J.M. TIBERIUS
Delft University of Technology, Delft, The Netherlands

The ambiguity-resolved detector (ARD) is developed for the validation of high-precision Global Navigation Satellite Systems (GNSS) mixed-integer observation models. The ARD releases the high success rate restriction of resolving the float ambiguities to integers, enabling ambiguity resolution to contribute to model validation even if the resolution success rate is not close to one. However, there are no closed-form expressions for the distribution of the ARD test statistic. The ARD critical value can only be obtained by Monte Carlo simulation, which requires heavy computations. To reduce the effort of applying the ARD, we provide a lookup table for the critical value of the ARD that utilizes the integer least-squares (ILS) estimator to resolve the ambiguities (ARD_{ILS}). We obtain 263 408 ARD_{ILS} critical values corresponding to GNSS observation models that vary in the precision of observables, satellite geometry, constellation, and the number of signal frequencies. We treat critical values as functions of the integer bootstrapping success rate and conduct curve fitting with second-order polynomials. The polynomial parameters are provided in the lookup table with which the ARD_{ILS} critical values can be simply computed rather than simulated. Numerical experiments demonstrate that the critical values computed with the lookup table provide significance levels close to the specified ones. The ARD_{ILS} can be implemented easily and efficiently with the lookup table. The lookup table with the polynomial coefficients to compute the ARD critical values can be downloaded from (Yin, 2024).

Received 26 November 2024; revised 14 March 2025, 8 May 2025, and 11 August 2025; accepted 17 August 2025. Date of publication 12 November 2025; date of current version 26 December 2025.

DOI. No. 10.1109/TAES.2025.3632272

Refereeing of this contribution was handled by S. Khanafseh.

The work of Chengyu Yin's was supported by the Dutch Research Council (NWO) through the "I-GNSS positioning for assisted and automated driving" project (18305). Dutch national e-infrastructure Snellius supercomputer was used with the support of the SURF Cooperative under Grant EINF-7002.

Authors' addresses: Chengyu Yin and Christian C.J.M. Tiberius are with the Delft University of Technology, Delft, The Netherlands, E-mail: (c.yin@tudelft.nl; c.c.j.m.tiberius@tudelft.nl). Peter J.G. Teunissen is with the Delft University of Technology, Delft, The Netherlands, and also with Curtin University, Perth, Australia, E-mail: (p.j.g.teunissen@tudelft.nl). *(Corresponding author: Chengyu Yin.)*

I. INTRODUCTION

Model validation is important for the data processing of Global Navigation Satellite Systems (GNSS). The assumed observation model can be misspecified by the unmodeled effects, for instance, outliers due to multipath, phase cycle slips, and atmosphere delays caused by abnormal weather conditions [2], [3], [4]. The parameter estimation will be biased if these effects remain unnoticed and the misspecified model is used [5], [6]. Misspecification detection is the first step in model validation, which is typically based on the overall model test through the norm of the residual vector [7], [8]. If the detection outcome indicates that the assumed model is not valid, identification tests can be conducted as the next step to identify the error contained in the observables.

The GNSS observation model for high-precision applications contains the unknown integer-valued carrier phase ambiguities alongside the real-valued unknowns such as user position coordinates [9], [10]. Three types of detectors can be used to detect a misspecification of the GNSS mixed-integer model: the ambiguity-known detector (AKD), ambiguity-float detector (AFD), and ambiguity-resolved detector (ARD) [11]. AKD can be applied if the ambiguities are deterministically *known* and can be removed from the vector of unknowns. It is more frequent in practice that the ambiguities are estimated instead of being known. If the integer property of the ambiguities is not considered, the AFD can be applied as if the ambiguities are *real-valued unknowns*. The ARD treats the ambiguities as *integer-valued unknowns* and is based on ambiguity resolution [11]. Yin et al. [12] showed that the ARD can provide better detection performance than the AFD, especially for detecting atmospheric delays, even if the ambiguity resolution success rate is not close to one. Therefore, ARD enables ambiguity resolution to be conducted and contribute to model validation under lower success rate cases.

The key step to conduct the ARD is ambiguity resolution [13], where the float ambiguities are resolved to integers with an integer estimator, for instance, integer rounding (IR), integer bootstrapping (IB) or integer least-squares (ILS) [14]. The probability of resolving the float ambiguities to the correct integer vector is known as the ambiguity resolution success rate [15]. Among all members of the integer estimators, the ILS estimator provides the highest success rate [16]; thus, the ARD employing the ILS estimator to resolve the ambiguities has best detection performance. Due to the discrete nature of the resolved ambiguities, there are no closed-form expressions for the distribution of the ARD test statistic [11]. As a result, the ARD critical value can only be obtained by Monte Carlo simulation [17], which requires a heavy computational burden and hinders application of the ARD in real-time.

To reduce the effort of applying the ARD, we provide a lookup table for the critical value of the ARD employing the ILS estimator (ARD_{ILS}). The ARD_{ILS} critical value is entirely driven by the observation model and can be obtained without collecting the GNSS observations. Based on real satellite ephemeris, we formulate GNSS observation models that vary in the precision of observables, satellite geometry, constellation, and the number of signal frequencies. Then, we obtain the ARD_{ILS} critical values for these models through Monte Carlo simulation. We find that the ARD_{ILS} critical values can be considered as functions of the IB success rate of the ambiguity resolution. We conduct curve fitting with second-order polynomials and provide the polynomial parameters in the lookup table. With the number of frequencies and redundancy of the observation model as indexes, the coefficients of the second-order polynomial can be found in the lookup table, with which the ARD_{ILS} critical value can easily be computed as a function of the IB success rate. The critical value of the detection is typically chosen to fulfill a user-specified significance level, α. The significance level used by GNSS model validation varies in applications and the typical values are $\alpha = 0.1\%$ [18], [19], $\alpha = 0.5\%$ [20], and $\alpha = 5\%$ [21], [22]. Therefore, the lookup table provided in this contribution covers the significance levels $\alpha = [0.1\%, 0.5\%, 1\%, 5\%]$. The lookup table is provided in the 4TU research database [1].

The rest of this article is organized as follows. Section II reviews the ambiguity resolution and detection theory for the GNSS mixed-integer model. The procedure to obtain the ARD_{ILS} critical value by Monte Carlo simulation is described in Section III, in which also an example is presented to show the relation between the number of simulation samples, computation time and uncertainty of the simulated critical value. Section IV introduces how we generate the lookup table and explains how to use it. Section V shows experiments to evaluate the performance of the lookup table. Finally, Section VI concludes this article.

We use the following notations: $\mathbb{R}^m$ and $\mathbb{Z}^n$ denote the m-dimensional real space and the n-dimensional integer space, respectively. $E\{\cdot\}$ and $D\{\cdot\}$ refer to the expectation and dispersion operator. An underlined symbol indicates a random variable vector, e.g., $\underline{x}$. $\mathcal{N}_m(x, Q)$ is an m-dimensional normal distribution with mean x and variance–covariance (VC) matrix Q. $M^+ = (M^T Q^{-1} M)^{-1} M^T Q^{-1}$ refers to the BLUE (best linear unbiased estimator) inverse of matrix M. $P_M = MM^+$ is the orthogonal projector that projects onto the range space of M and $P_M^\perp = I - P_M$ projects to the null space of M. $||\cdot||_Q^2 = (\cdot)^T Q^{-1}(\cdot)$ presents the weighted squared norm of a vector. $\mathbf{1}_k$ denotes a $k \times 1$ vector with values of 1 and I_k is a k-dimensional identity matrix. $[\cdot]$ refers to the rounding operation. $\otimes$ denotes the Kronecker product.

II. REVIEW OF THEORY

The ARD is developed for validating the GNSS mixed integer observation model, which can be written as [9], [10]

$$\mathcal{H}_0: \quad E\{\underline{y}\} = Aa + Bb, \quad D\{\underline{y}\} = Q_{yy} \tag{1}$$

where $\mathcal{H}_0$ refers to the model under the nominal condition (null hypothesis); $\underline{y} = [\underline{\phi}^T, \underline{p}^T]^T \sim \mathcal{N}_m(E\{\underline{y}\}, Q_{yy})$ is the m-vector containing the carrier phase $\underline{\phi}$ and pseudorange $\underline{p}$ observables, which are assumed to be normally distributed. $a \in \mathbb{Z}^n$ contains the unknown integer-valued ambiguities and $b \in \mathbb{R}^p$ contains real-valued unknowns, e.g., the user position coordinates. $[A, B]^{m\times(n+p)}$ is the design matrix of full column rank.

This section will first review the ambiguity resolution theory, which is the key step in computing the ARD test statistic. Then, the detection theory for the GNSS mixed-integer model (1) will be introduced. Finally, the short-baseline double-differenced model will be presented, which is used to generate the lookup table for the ARD critical values.

A. Ambiguity Resolution

GNSS carrier phase ambiguity resolution is the key step to computing the ARD test statistic. It starts with ignoring the integer property of the ambiguities to obtain the float ambiguity estimator [23]

$$\underline{\hat{a}} = \bar{A}^+ \underline{y}, \quad Q_{\hat{a}\hat{a}} = \left(\bar{A}^T Q_{yy}^{-1} \bar{A}\right)^{-1} \tag{2}$$

with $\bar{A} = P_B^\perp A$. The float ambiguity vector can be resolved to an integer vector with one of the integer estimators [14], such as the IR, IB, and ILS, denoted as $\underline{\check{a}} = \mathcal{I}(\underline{\hat{a}})$, with $\mathcal{I}: \mathbb{R}^n \to \mathbb{Z}^n$. Before applying an integer estimator to resolve the ambiguities, a decorrelation transformation should be applied to the float ambiguities, which can increase the success rate of the IR and IB, as well as the efficiency of the ILS [23], [24]. The ILS estimator is used in this contribution to resolve the ambiguities

$$\underline{\check{a}}_{ILS} = \arg\min_{z\in\mathbb{Z}^n} \|\underline{\hat{a}} - z\|_{Q_{\hat{a}\hat{a}}}^2 \tag{3}$$

which is the integer vector nearest to the float ambiguity vector under the metric of $Q_{\hat{a}\hat{a}}$. It can be obtained efficiently with the LAMBDA method [23], [25].

The success rate of the ILS estimator can not be computed analytically [16]. In this contribution, we use the IB success rate $P_{\text{SR,IB}}$ as an approximation, which is a tight and easy-to-compute lower bound of the ILS success rate [15], [26]

$$P_{\text{SR,IB}} = P(\check{a}_{\text{IB}} = a) = \prod_{i=1}^{n} \left[2\Phi\left(\frac{1}{2\sigma_{\hat{a}_{i|I}}}\right) - 1\right] \tag{4}$$

where $\check{a}_{\text{IB}}$ denotes the resolved ambiguity vector with the IB estimator; a is the correct ambiguity vector; the conditional standard deviations $\sigma_{\hat{a}_{i|I}}$, with I denotes $1, \ldots, i-1$, are the square roots of the diagonal values of matrix D obtained from the triangular matrix factorization $Q_{\hat{a}\hat{a}} = LDL^T$; $\Phi(x)$ is the cumulative distribution function (CDF) of the standard normal distribution.

The ambiguity residual vector is a key component of the ARD test statistic. It is defined as the difference between the float and the resolved ambiguity estimator

$$\underline{\check{\epsilon}} = \underline{\hat{a}} - \underline{\check{a}}. \tag{5}$$

The distribution of $\underline{\check{e}}$ under $\mathcal{H}_0$ is [27]

$$f_{\underline{\check{e}}}(x) = \frac{\sum_{z\in\mathbb{Z}^n} \exp\{-\frac{1}{2}\|x+z\|^2_{Q_{\hat{a}\hat{a}}}\}}{\sqrt{|2\pi Q_{\hat{a}\hat{a}}|}} s_0(x) \tag{6}$$

with $s_0(x)$ the indicator function of the so-called pull-in region of the zero vector, S_0,

$$s_0(x) = \begin{cases} 1 & x \in S_0 \\ 0 & \text{otherwise.} \end{cases} \tag{7}$$

As $\mathcal{I} : \mathbb{R}^n \to \mathbb{Z}^n$ is a many-to-one mapping, different float ambiguity vectors can be resolved to the same integer vector. The pull-in region S_0 is the set containing all the float vectors $\hat{a} \in \mathbb{R}^n$ resolved to the zero vector [13]. The distribution $f_{\underline{\check{e}}}(x)$ is an infinite sum of shifted normal distributions truncated into S_0.

B. Detection Theory

The AFD, AKD, and ARD can be used for GNSS mixed-integer model validation [11]. The AFD is applied when ambiguity resolution is not conducted. The AKD can be utilized if the ambiguities are deterministically known. The ARD is based on the *resolved* ambiguities. For parameter estimation, ambiguity resolution is conducted only when the success rate is sufficiently close to one to avoid the bias caused by wrongly resolved ambiguities. For model validation, this restriction can be released as the ARD can provide better performance than the AFD in the lower success rate cases [11], [12].

The detectors are formulated based on the corresponding residuals

$$\begin{aligned} \text{AF: } & \underline{\hat{e}} = P^{\perp}_{[A,B]}\underline{y} \\ \text{AK: } & \underline{\hat{e}}(a) = P^{\perp}_{B}(\underline{y} - Aa) \\ \text{AR: } & \underline{\check{e}} = \underline{\hat{e}}(\underline{\check{a}}) = P^{\perp}_{B}(\underline{y} - A\underline{\check{a}}). \end{aligned} \tag{8}$$

The test statistics of these detectors are the square norms of the corresponding residuals. The AFD and AKD test statistics and their distributions under $\mathcal{H}_0$ are written as

$$\begin{aligned} &\text{AFD: } \|\underline{\hat{e}}\|^2_{Q_{yy}} \mid \mathcal{H}_0 \sim \chi^2(r,0) \\ &\text{AKD: } \|\underline{\hat{e}}(a)\|^2_{Q_{yy}} \mid \mathcal{H}_0 \sim \chi^2\left(r(a),0\right) \end{aligned} \tag{9}$$

where $r = m - n - p$ and $r(a) = m - p$ are the model redundancies when the ambiguities are unknown and known, respectively. The ARD test statistic can be written with ambiguity residual vector (5) as

$$\|\underline{\check{e}}\|^2_{Q_{yy}} = \|\underline{\hat{e}}\|^2_{Q_{yy}} + \|\underline{\check{\epsilon}}\|^2_{Q_{\hat{a}\hat{a}}}. \tag{10}$$

Its distribution can not be written in a closed-form expression since the distribution of $\underline{\check{\epsilon}}$ (6) is truncated by the ambiguity pull-in region [11]. Compared with the AFD test statistic, it contains the squared norm of $\underline{\check{\epsilon}}$ additionally; thus, ambiguity resolution also contributes to detecting the model misspecifications.

With the test statistics and the user-specified significance level α, these three detectors are written as follows:

$$\begin{aligned} &\text{AFD: Reject } \mathcal{H}_0 \text{ if } \|\underline{\hat{e}}\|^2_{Q_{yy}} > \chi^2_\alpha(r,0) \\ &\text{AKD: Reject } \mathcal{H}_0 \text{ if } \|\underline{\hat{e}}(a)\|^2_{Q_{yy}} > \chi^2_\alpha\left(r(a),0\right) \\ &\text{ARD: Reject } \mathcal{H}_0 \text{ if } \|\underline{\check{e}}\|^2_{Q_{yy}} > \kappa_\alpha. \end{aligned} \tag{11}$$

Here, $\chi^2_\alpha(r,0)$ and $\chi^2_\alpha(r(a),0)$ are the AFD and AKD critical values obtained based on the CDF of the central chi-squared distributions with degrees of freedom r and $r(a)$, respectively. The ARD critical value κ_α can only be obtained by Monte Carlo simulation [17]. The detailed simulation procedure and an example are provided in Section III.

Teunissen [11] showed that the distribution of the ARD test statistic lies between those of the AFD and AKD. The more precise the ambiguities become, the more the ARD will behave like the AKD. On the other hand, the ARD will then behave similarly to the AFD when ambiguities get less precise. It follows that their critical values fulfill the relation $\chi^2_\alpha(r,0) \le \kappa_\alpha \le \chi^2_\alpha(r(a),0)$.

C. Observation Model

Single-epoch short-baseline double-differenced observation models are used to obtain the AR critical values to create the lookup table. The lookup table can also be used with single-epoch undifferenced and single-differenced short baseline observation models, as well as atmosphere-corrected network RTK and PPP-RTK user models, given that the vc matrix of the corrections is appropriately considered. These models are intrinsically equivalent to the double-differenced model and provide the same model redundancy and estimators for user position and ambiguities under the same observation setup [28], [29].

Assume s satellites from a single constellation are tracked on f frequencies for a single epoch. The design matrix for the ambiguity vector is

$$A = \begin{bmatrix} 1 & 0 \end{bmatrix}^T \otimes \text{diag}(\lambda_1, \ldots, \lambda_f) \otimes I_{s-1} \tag{12}$$

where λ_f is the wavelength of the fth frequency. The design matrix for the baseline vector is

$$B = \mathbf{1}_2 \otimes \mathbf{1}_f \otimes (D^T G) \tag{13}$$

with $D^T = \begin{bmatrix} -\mathbf{1}_{s-1} & I_{s-1} \end{bmatrix}$ the $(s-1)\times s$ differencing matrix and G the $s \times 3$ geometry matrix contains the unit vectors from satellites to the receiver. The vc matrix of $\underline{y}$ is

$$Q_{yy} = \begin{bmatrix} \sigma^2_\phi & \\ & \sigma^2_p \end{bmatrix} \otimes I_f \otimes 2D^T W^{-1} D. \tag{14}$$

Here, σ_ϕ and σ_p are the zenith-referenced undifferenced phase and pseudorange standard deviations; we assume the phase and pseudorange observables to be uncorrelated. With

the identity matrix I_f, we assume the observables from different frequencies to be uncorrelated and of the same precision. $W = \mathrm{diag}(w_1, \ldots, w_i, \ldots, w_s)$ is a diagonal matrix contains the elevation-dependent weights [30]

$$w_i = 1/\left(a_0 + a_1 \exp\left(-\frac{E^i}{E_0}\right)\right)^2 \tag{15}$$

where E^i is the elevation of the ith satellite in degrees; a_0, a_1, and E_0 are receiver-dependent parameters and they are set as 1, 10, and 10° in our computation. Although a specific stochastic model setup is used to create the lookup table, the table remains applicable to users with different stochastic model configurations. As will be shown later, the critical value is computed as a function of the IB failure rate, which inherently accounts for variations in the stochastic model.

For the observation model with observables from two constellations, the design matrices and vc-matrices are stacked as follows:

$$A = \begin{bmatrix} A^1 \\ & A^2 \end{bmatrix}, B = \begin{bmatrix} B^1 \\ B^2 \end{bmatrix}, Q_{yy} = \begin{bmatrix} Q^1_{yy} \\ & Q^2_{yy} \end{bmatrix} \tag{16}$$

where A^i, B^i, and Q^i_{yy} are the design matrix and vc-matrix of the ith ($i = 1, 2$) constellation.

III. ARD CRITICAL VALUE

In this section, we first describe the procedure to simulate the ARD critical value numerically. Then, an example is presented to show the relation between the number of samples, simulation uncertainty, and computation time.

A. Simulation Procedure

The critical value of the ARD fulfills

$$\int_0^{\kappa_\alpha} f_{\|\check{\underline{e}}\|^2_{Q_{yy}}}(x)dx = 1 - \alpha \tag{17}$$

which can be obtained through Monte Carlo quantile simulation [31], as there are no closed-form expressions for the distribution of $\|\check{\underline{e}}\|^2_{Q_{yy}}$. According to (10) and the independence between $\hat{\underline{e}}$ and $\check{\underline{e}}$ [11], we can generate samples of $\|\hat{\underline{e}}\|^2_{Q_{yy}}$ and $\|\check{\underline{e}}\|^2_{Q_{\hat{a}\hat{a}}}$ independently and then obtain samples of $\|\check{\underline{e}}\|^2_{Q_{yy}}$. Following the "remove–restore" property of the integer estimator [16], samples of the ambiguity residual $\check{\underline{e}}$ can be obtained without knowing the true ambiguity vector, and we can use $a = 0$ to conduct the simulation. Assuming we use N samples in Monte Carlo simulation, the ARD critical value can be obtained as follows.

1) Generate N samples of the float ambiguity vector $\hat{a}^{(1)}, \ldots, \hat{a}^{(i)}, \ldots, \hat{a}^{(N)}$, that follow the normal distribution $\mathcal{N}_n(0, Q_{\hat{a}\hat{a}})$.
2) Resolve the float ambiguity samples $\hat{a}^{(i)}$ with one of the integer estimators [14], and obtain samples of the resolved ambiguity vector $\check{a}^{(1)}, \ldots, \check{a}^{(i)}, \ldots, \check{a}^{(N)}$.
3) Generate samples of $\|\hat{\underline{e}}\|^2_{Q_{yy}}$ that follow $\chi^2(r, 0)$, denoted as $\|\hat{e}\|^{2,(1)}_{Q_{yy}}, \ldots, \|\hat{e}\|^{2,(i)}_{Q_{yy}}, \ldots, \|\hat{e}\|^{2,(N)}_{Q_{yy}}$.

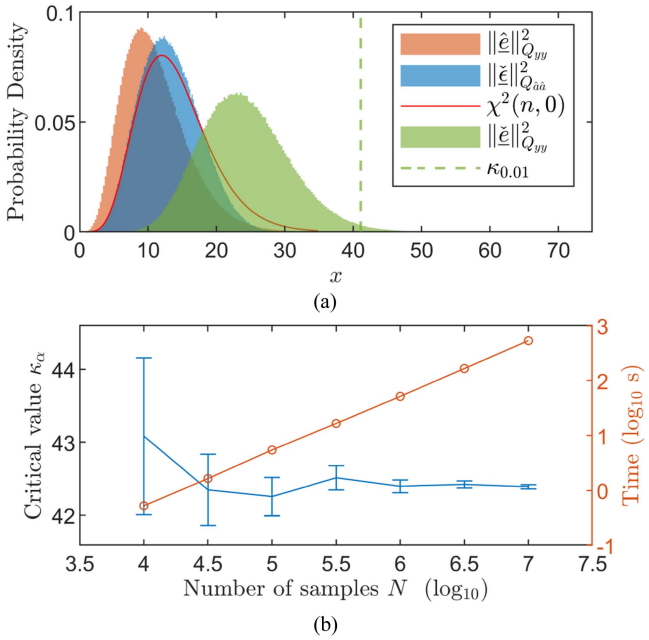

Fig. 1. Example of AR critical value simulation. (a) Normalized histograms of samples and critical value for $\alpha = 0.01$. (b) Simulated critical value with 99% confidence interval (vertical bars in blue) and computation times (in orange).

4) According to (10), samples of the ARD test statistic can then be computed as

$$\|\check{e}\|^{2,(i)}_{Q_{yy}} = \|\hat{a}^{(i)} - \check{a}^{(i)}\|^2_{Q_{\hat{a}\hat{a}}} + \|\hat{e}\|^{2,(i)}_{Q_{yy}}.$$

5) Finally, sort the samples $\|\check{e}\|^{2,(i)}_{Q_{yy}}$ in ascending order, the $[(1-\alpha)N]^{th}$ ordered sample is taken as the critical value.

In our computations, the ILS estimator is used to resolve the ambiguity in step 2) to obtain samples of the $\mathrm{ARD}_{\mathrm{ILS}}$ critical value.

B. Numerical Example

An example of $\mathrm{ARD}_{\mathrm{ILS}}$ critical value simulation is shown in Fig. 1, which is based on a single-epoch dual-frequency double-differenced observation model with eight GPS satellites, $r = 11$, $n = 14$, and the ILS success rate approximates 78%.

Fig. 1(a) shows the normalized histograms of 10^6 samples of $\|\hat{\underline{e}}\|^2_{Q_{yy}}$ (orange), $\|\check{\underline{e}}\|^2_{Q_{\hat{a}\hat{a}}}$ (blue) and $\|\check{\underline{e}}\|^2_{Q_{yy}}$ (green); normalization is conducted such that values of the histograms represent probability densities. The vertical line in green gives the $\mathrm{ARD}_{\mathrm{ILS}}$ critical value for $\alpha = 0.01$. The red curve shows the PDF of $\chi^2(n, 0)$, which is the distribution of $\|\hat{\underline{a}} - a\|^2_{Q_{\hat{a}\hat{a}}}$ with the known ambiguity vector. The histogram of $\|\check{\underline{e}}\|^2_{Q_{\hat{a}\hat{a}}}$ is different from $\chi^2(n, 0)$ as is shown in the figure. Hence, when applying the $\mathrm{ARD}_{\mathrm{ILS}}$, the resolved ambiguity vector cannot be assumed to be a known vector.

Fig. 1(b) provides the simulated $\mathrm{ARD}_{\mathrm{ILS}}$ critical value for $\alpha = 0.01$ in blue and computation time as functions of the number of samples in orange. The vertical

TABLE I
Model Configurations to Obtain ARD Critical Value Dataset

Constellation	Single-Fre.	Dual-Fre.	Triple-Fre.
GPS	L1	L1/L5	L1/L5/L2
Galileo	E1	E1/E5a	E1/E5a/E5b
GPS+Galileo	L1+E1	L1/L5+ E1/E5a	L1/L5/L2+ E1/E5a/E5b

error bar shows the 99% confidence interval for each simulation, which is obtained based on the asymptotic normality of the simulated critical value, following the method described in [12] and [31]. The computation time in seconds corresponds to a 3.6 GHz single CPU core. Fig. 1(b) shows that simulating the critical value with a tight confidence interval requires tens of seconds, which blocks the application of the ARD_{ILS} detector for real-time applications.

IV. LOOKUP TABLE GENERATION

In order to apply the ARD, we need to compute the critical value κ_α for the given observation model and specified significance level. In Section III, we described a simulation-based approach to obtain κ_α as it cannot be computed analytically, but the experiment also shows that the simulation is time-consuming. Hence, it is of interest to investigate whether there is a relation between the observation model parameters and κ_α such that it can be computed easily based on the model parameters. This section shows that this relation exists and describes how we create the lookup table for κ_α.

A. Dataset

The ARD_{ILS} critical value κ_α is fully driven by the observation model and can be computed without collecting actual GNSS observations. To investigate the relation between the GNSS observation model parameters and the ARD_{ILS} critical value κ_α, we first prepare a dataset with in total 263 408 critical values κ_α for significance levels $\alpha = [0.1\%, 0.5\%, 1\%, 5\%]$, obtained with GNSS observation models that are different in configuration, observable precision and satellite geometry.

For model configurations, we use single-, dual- and triple frequency models with single- and dual-constellation, which are summarized in Table I. In terms of observable precision, we fix the ratio $\sigma_p/\sigma_\phi = 100$ and change σ_p from 0.1 m to 1.0 m to cover the precision of different types of the receivers [32], [33], [34]. Regarding satellite geometries, we consider nine receiver locations with different latitudes. Since the observed GNSS satellite geometry is affected by the latitude, the locations' longitudes are all fixed to 0°, and the latitude increases from 0° to 80° with a 10° interval. We formulate 288 single-epoch short-baseline double-differenced observation models at each location based on the satellite orbit product from the International GNSS Service [35] every 5 min for 24 h.

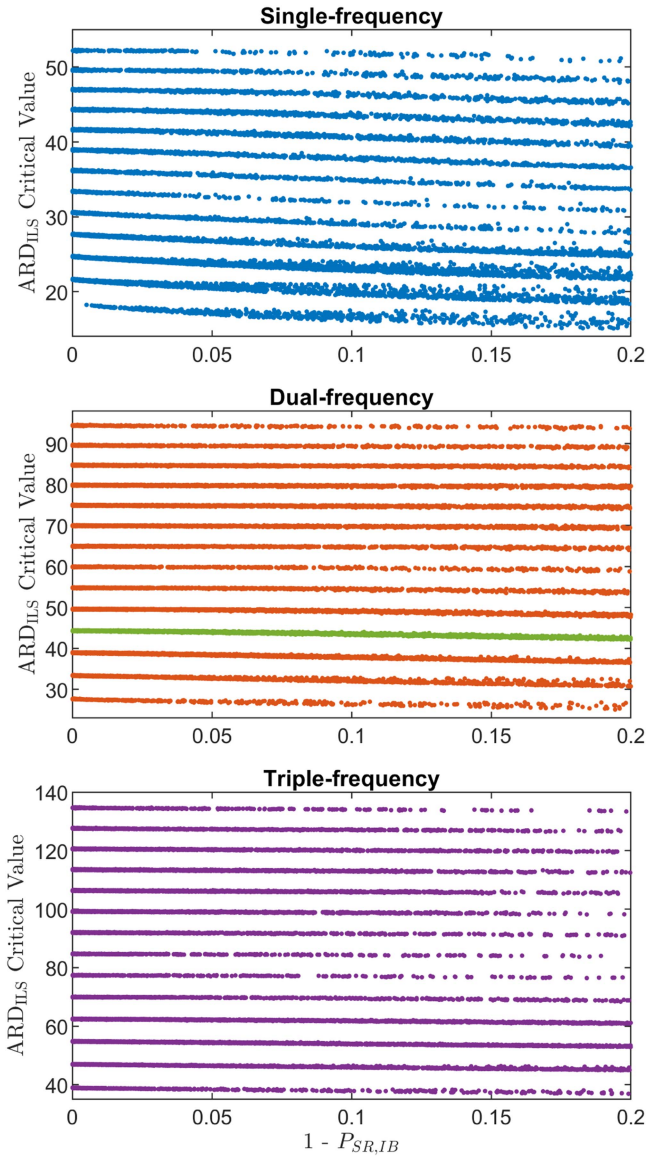

Fig. 2. ARD_{ILS} critical value dataset for significance level $\alpha = 1\%$ plotted as a function of IB failure rate $1 - P_{\text{SR,IB}}$. Each curve is associated with a specific $r(a)$ listed in Table II. For example, dual-frequency curve in *green* contains 5293 critical values corresponding to observation models with $r(a) = 25$ and eight satellites, as is highlighted in Table II.

For each model, κ_α is obtained through Monte Carlo simulation with 10^6 samples. The models with the IB success rate $0.8 < P_{\text{SR,IB}} < 0.9999$ are taken into account because i) ARD_{ILS} performs similarly to the AFD when the success rate $P_{SR,IB}$ is lower than 0.8 [12] and it is not of interest to be used ii) κ_α will be very close to the AKD critical value for $P_{\text{SR,IB}} \geq 0.9999$ and the lookup table is not needed in this case.

To analyze the relation between the ARD_{ILS} critical value and the model parameters, we plot critical values in the dataset as a function of the IB failure rate, $1 - P_{\text{SR,IB}}$, as is shown in Fig. 2. The reason for this visualization is as follows. The distribution of the ARD_{ILS} test statistic changes with the precision of the float ambiguity estimator [11],

TABLE II
Summary of Dataset for ARD_{ILS} Critical Value

Single-constellation	s	**5**	**6**	**7**	**8**	**9**	**10**	**11**							
Dual-constellation	s						**11**	**12**	**13**	**14**	**15**	**16**	**17**	**18**	**19**
Single-frequency	$r(a)$		**7**	**9**	**11**	**13**	**15**	**17**	**19**	**21**	**23**	**25**	**27**	**29**	**31**
	#CV		589	2160	2857	1932	851	394	771	1316	1473	1392	1017	573	266
Dual-frequency	$r(a)$	**13**	**17**	**21**	**25**	**29**	**33**	**37**	**41**	**45**	**49**	**53**	**57**	**61**	**65**
	#CV	486	2116	4292	5293	3345	1323	637	1315	2152	2405	2278	1637	914	408
Triple-frequency	$r(a)$	**21**	**27**	**33**	**39**	**45**	**51**	**57**	**63**	**69**	**75**	**81**	**87**	**93**	**99**
	#CV	545	2145	3237	2766	858	370	430	1257	2128	2463	2335	1729	974	423

Dataset considers observation models with $0.8 < P_{\text{SR,IB}} < 0.9999$. Ambiguity-known redundancies $r(a)$ for models with different numbers of frequencies, observed satellites (s), and constellations are listed. The numbers of critical values (#CV) contained in the dataset are provided below the corresponding $r(a)$. Each pair of $r(a)$ and #CV is associated with one curve in Fig.2, e.g., dual-frequency model with $r(a) = 25$ highlighted in green above corresponds to green curve in dual-frequency graph of Fig. 2.

which is determined by the $n \times n$ matrix $Q_{\hat{a}\hat{a}}$, and so does the critical value κ_α. As it is not convenient to compute κ_α on the basis of the full $Q_{\hat{a}\hat{a}}$ matrix, we use $1 - P_{\text{SR,IB}}$, which is a scalar measure of the ambiguity precision and easy-to-compute.

As is shown in Fig. 2, the ARD_{ILS} critical values κ_α cluster onto 13 curves in the single-frequency graph and 14 curves in the dual- and triple-frequency graphs and each curve can apparently be considered a function of $1 - P_{\text{SR,IB}}$. Each curve corresponds to one specific ambiguity-known redundancy $r(a)$. Because the distribution of the ARD_{ILS} test statistic will be the same as that of the AKD when the float ambiguity estimator is very precise, $1 - P_{\text{SR,IB}} = 0$, and κ_α will be the same as the AKD critical value $\chi^2_\alpha(r(a), 0)$. As a result, each curve starts on the left from $\chi^2_\alpha(r(a), 0)$ with a certain $r(a)$ and decreases with the increase of the IB failure rate.

Table II summarizes the ambiguity-known redundancies $r(a)$ and the number of critical values **#CV** contained in the dataset. As we observed in Fig. 2, critical values κ_α cluster onto curves corresponding to ambiguity-known redundancy $r(a)$. Table II lists all the $r(a)$ associated with Fig. 2. $r(a)$ is determined by the number of observed satellites s and the number of signal frequencies f in the observation model. For a single-epoch single-constellation double-differenced model with pseudorange and carrier phase observables, $r(a) = 2f(s-1) - 3$, and $r(a) = 2f(s-2) - 3$ for the dual-constellation model with in total s satellites from two constellations as each constellation needs a reference satellite. The 13 $r(a)$ values in the first row of the table coincide with the 13 curves in the single-frequency plot in Fig. 2. Similarly, 14 $r(a)$ values in the table are associated with the 14 curves in Fig. 2 for dual and triple-frequency models. For example, the green curve in the dual-frequency graph in Fig. 2 is associated with the element in Table II highlighted in green. This curve assembles κ_α for the dual-frequency observation models with eight observed satellites and $r(a) = 25$. In the single-frequency case, a model with 5 satellites is very weak, and $P_{\text{SR,IB}}$ is typically smaller than 0.8 even with very precise observables; thus, this case is not included in the dataset. The number of the critical values **#CV** for each $r(a)$ is also provided in the table, which is the number of data points on the corresponding curve in Fig. 2.

B. Indexes of Lookup Table

By plotting the ARD_{ILS} critical values κ_α as a function of IB failure rate $1 - P_{\text{SR,IB}}$, it is shown in Fig. 2 that the critical values κ_α cluster onto distinct curves. According to this observation, we create a lookup table in two steps. First, we decide on the lookup table indexes to determine which curve κ_α lies on. Then, we conduct curve fitting and provide the fitting coefficients for each curve, and the critical value can be computed as a function of the IB failure rate $1 - P_{\text{SR,IB}}$. In this section, we discuss which parameters should be used as the lookup table indexes.

As is shown in Fig. 2, even though the critical values are generated at different user locations, with different satellite constellations, geometries, and precision of observables, they lie on distinct curves associated with the ambiguity-known model redundancy $r(a)$. Therefore, $r(a)$ should be one of the lookup table indexes.

The critical values are also driven by the significance level α, an example with the dual-frequency model, $r(a) = 25$ and four significance levels is shown in Fig. 3. The curves are shifted to start from zero by subtracting the corresponding AKD critical values to compare their shapes clearly. It is shown that the critical values for different α decrease differently. Hence, the specified α should also be a lookup table index.

The dependency of the curves' shape on the number of frequencies of the model f is checked in Fig. 4, where two examples are provided. Each example contains two curves with models of the same $r(a)$ but different f. It shows that the critical value for models of different f can decay differently even if they have the same $r(a)$. Therefore, f should be another lookup table index.

With the specified significance level α, ambiguity-known redundancy $r(a)$, and the number of frequencies f of the model, one can determine which curve the ARD_{ILS}

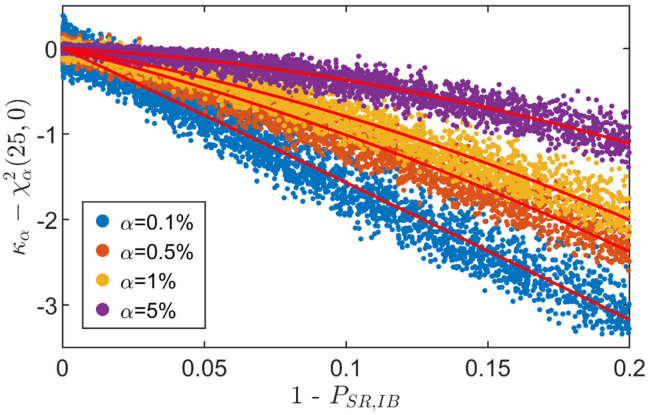

Fig. 3. $\kappa_\alpha - \chi^2_\alpha(25,0)$ as a function of $1 - P_{\text{SR,IB}}$ for dual-frequency model $r(a) = 25$ with four significance levels. The AKD critical value $\chi^2_\alpha(25,0)$ is subtracted from κ_α to compare the curves' shapes. Red lines are fitted second-order polynomials.

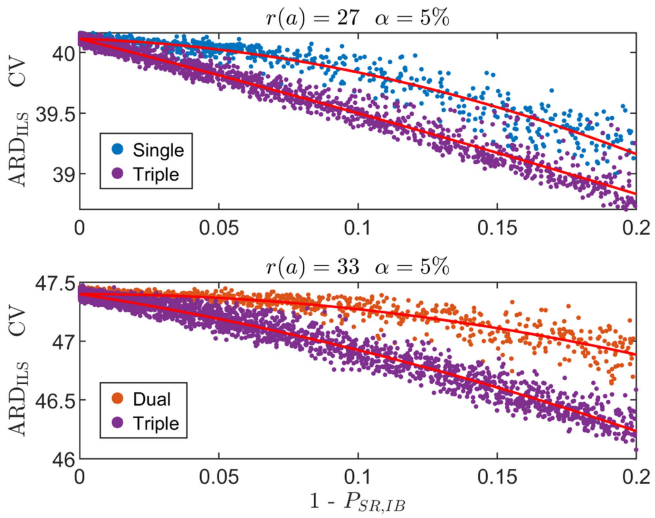

Fig. 4. Critical values for same $r(a)$ and different numbers of frequencies as a function of $1 - P_{\text{SR,IB}}$. Red lines are fitted with second-order polynomials.

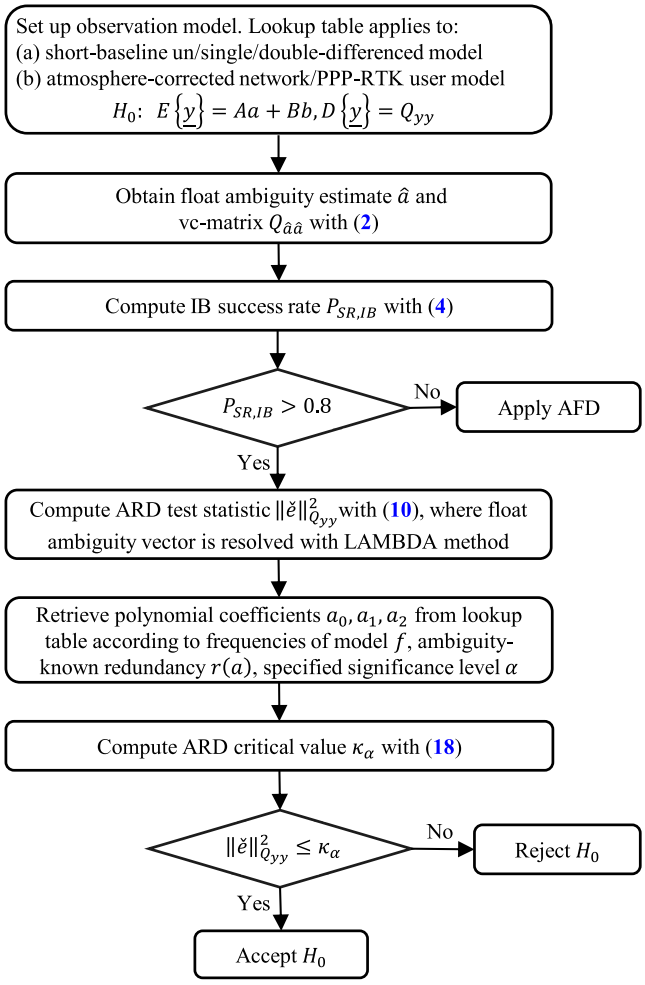

Fig. 5. Steps to use ARD based on lookup table.

critical value lies on. These three parameters are the lookup table indexes for the ARD_{ILS} critical value.

C. Curve Fitting

After determining the three lookup table indexes, we conduct curve fitting to fit the curves as a function of the IB failure rate. The detailed plots of the curves in Figs. 3 and 4 show that the shape of the curve is smooth but nonlinear. We fit the curves with second-order polynomials, which can fit the shape of the curve very well. Curve fitting is conducted using the following model:

$$k_\alpha = a_0 + a_1 x + a_2 x^2 \tag{18}$$

with $x = 1 - P_{\text{SR,IB}}$; a_0 the AKD critical value $\chi^2_\alpha(r(a),0)$; a_1 and a_2 the polynomial coefficients to be determined. For $x = 0$, the critical value is constrained to $a_0 = \chi^2_\alpha(r(a),0)$. Curve fitting is conducted with unweighted least-squares. Examples of the fitted curves are shown in Figs. 3 and 4 in red, demonstrating that the curves, with the three aforementioned indices, as functions of the IB failure rate, well fit the critical value data points.

D. Use ARD With Lookup Table

The lookup table can be found at the research database [1], which contains the coefficients a_0, a_1, and a_2 of all $r(a)$ included in Table II for significance levels $\alpha = [0.1\%, 0.5\%, 1\%, 5\%]$.

The steps to use the ARD based on the lookup table provided in this contribution are described in Fig. 5. After obtaining the float ambiguity estimate and the corresponding vc-matrix $Q_{\hat{a}\hat{a}}$ with (2), the IB success rate can be computed with (4). The ARD can be applied with the lookup table if $P_{\text{SR,IB}}$ is larger than 80%. The float ambiguity vector should be resolved by the LAMBDA method, and the ARD test statistic $\|\check{e}\|^2_{Q_{yy}}$ is computed with (10). The polynomial coefficients can be retrieved from the lookup table with the specified significance level α, number of frequencies f and ambiguity-known redundancy $r(a)$ of the model as indexes, with which the ARD critical value κ_α is computed with (18) as a function of $P_{\text{SR,IB}}$. The model under $\mathcal{H}_0$ is accepted if $\|\check{e}\|^2_{Q_{yy}} \leq \kappa_\alpha$.

TABLE III
Locations to Evaluate the Lookup Table

Location	Latitude (°)	Longitude (°)	Elevation (m)
1	1.4	103.8	15
2	-15.8	-47.9	1100
3	30.6	114.3	37
4	-37.8	145	31
5	52	4.4	0
6	64.1	-21.9	0

It should be noted that the lookup table provided in this contribution applies to single-epoch GNSS short-baseline observation models or the atmosphere-corrected network/PPP-RTK user model. It does not apply to other GNSS high-precision observation models. For example, multiepoch models or models containing unknowns related to troposphere or ionosphere delays. Because these models have different redundancies, the critical value may decrease differently compared to the short-baseline model, even under the same observation configuration. We describe the general procedure to create a lookup table of the ARD critical value in Appendix A for users of interest to create lookup tables for different models.

V. PERFORMANCE EVALUATION

This section introduces how we evaluate the performance of the lookup table for the ARD_{ILS} critical value and shows the results of evaluation experiments.

We evaluate the performance of the lookup table by comparing the significance level of the critical value obtained through the lookup table α_{LT} with the specified significance level α. Experiments are carried out with three model configurations: the single-frequency GPS+Galileo, dual-frequency GPS, and triple-frequency Galileo models, over six user locations spread at different latitudes and elevations, as shown in Table III. Observation models are obtained with 288 satellite geometries over 24 h with a 5-min interval for each location and model configuration. α_{LT} are simulated for each observation model with Monte Carlo simulation employing $N = 2 \times 10^8$ samples. The steps to simulate α_{LT} with a given critical value are described in Appendix B. The simulation standard deviation varies from 2.2×10^{-6} for $\alpha_{LT} = 0.1\%$ to 1.5×10^{-5} for $\alpha_{LT} = 5\%$, computed with

$$\sigma_{\alpha_{LT}} = \sqrt{\frac{\alpha_{LT}(1-\alpha_{LT})}{N}}. \tag{19}$$

The simulation uncertainty is small compared with α_{LT} and is not considered when evaluating the performance of the lookup table.

Fig. 6 shows the experiment results at location 5. The ARD_{ILS} critical values are computed with the lookup table when $P_{\text{SR,IB}} > 0.8$, and the corresponding significance levels α_{LT} are evaluated with Monte Carlo simulation. The results with the single-frequency GPS+Galileo, dual-frequency GPS, and triple-frequency Galileo models are shown in blue, yellow, and purple dots, respectively. Generally, the significance level with the lookup table α_{LT} is within the $\pm 5\%$ range around the specified α, indicated by the dashed red horizontal lines.

The relative difference of α_{LT} with respect to the expected α is computed as $|\alpha_{LT} - \alpha|/\alpha$. The empirical CDFs of the relative differences for $\alpha = [0.1\%, 0.5\%, 1\%, 5\%]$, computed with experiments at all locations with all model configurations are shown in Fig. 7. For $\alpha = 5\%$, the relative differences are smaller than 3.3% in 95% of the experiments, and for $\alpha = 0.1\%$, the relative differences are smaller than 8.5% in 95% of the experiments.

In practice, the user may assume the resolved ambiguity to be known and use the AKD critical value $\chi^2_\alpha(r(a), 0)$ (11) as the ARD_{ILS} critical value. Fig. 8 compares α_{LT} and the significance levels of using the AKD critical values α_{AKD}. It shows that the AKD critical value provides a much lower significance level than the specified one, especially when the success rate is low. Since the AKD critical value is larger than the ARD_{ILS} critical value, the corresponding significance level is always lower than specified. In contrast, the critical value from the lookup table can provide significance levels close to the specified one. Fig. 8 indicates that the resolved ambiguity could not be assumed to be known while conducting the ARD, and the lookup table performs much better than using the AKD critical value.

VI. SUMMARY AND CONCLUSION

We introduced a lookup table for the critical value κ_α of the ARD employing the ILS estimator, ARD_{ILS}.

We first reviewed the three detectors for the validation of the GNSS mixed-integer observation model: the AFD, AKD, and ARD. Then, we introduced how to obtain κ_α by Monte Carlo simulation and showed the computation time of the simulation. To reduce the effort of applying the ARD_{ILS}, we developed a lookup table that can provide an approximation of κ_α. The lookup table was generated based on 263 408 critical values for observation models of different configurations and satellite geometries, with the ambiguity known model redundancy $r(a)$, number of frequencies f, and specified significance level α as table indexes. We described how to apply ARD_{ILS} with the lookup table and conducted experiments to evaluate the lookup table by computing the significance level corresponding to the lookup table critical value, α_{LT}. We compute the relative difference of α_{LT} with respect to the specified α. For $\alpha = 5\%$, the relative differences are smaller than 3.3% in 95% of the experiments, and for $\alpha = 0.1\%$, the relative differences are smaller than 8.5% in 95% of the experiments.

The lookup table provided in this contribution applies to the single-epoch short-baseline double-differenced model and its equivalences, using the ILS estimator to resolve the ambiguity vector. We described the general procedure to

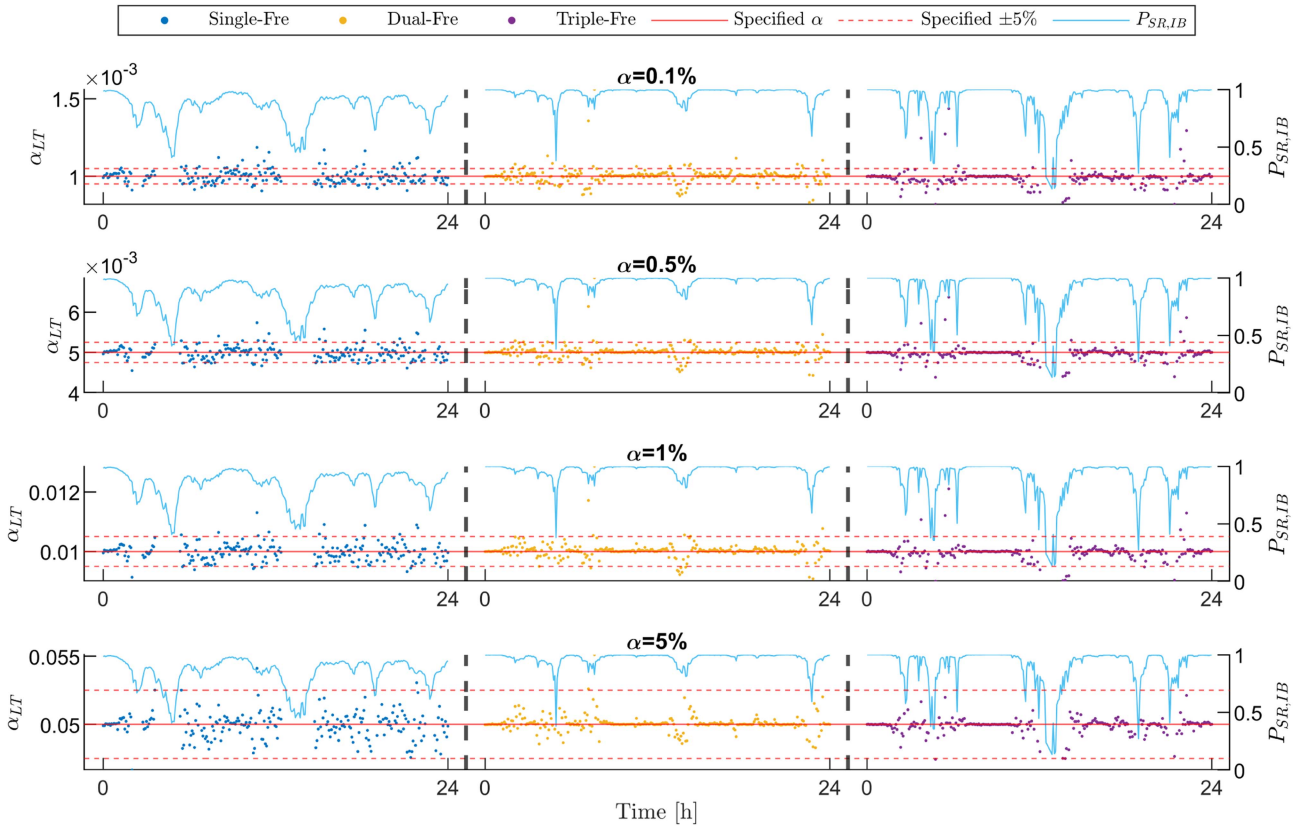

Fig. 6. Significance levels of critical values obtained with lookup table, α_{LT}, evaluated with single-frequency GPS+Galileo model (blue dots), dual-frequency GPS model (yellow dots), and triple-frequency Galileo model (purple dots) for four significance levels $\alpha = [0.1\%, 0.5\%, 1\%, 5\%]$. Observation models for each configuration are obtained on location 5 over 24 hours (288 epochs with a 5-min interval). Solid red horizontal line gives specified α, and dashed red lines show $(1 \pm 5\%)\alpha$. The cyan curve is IB success rate $P_{\mathrm{SR,IB}}$.

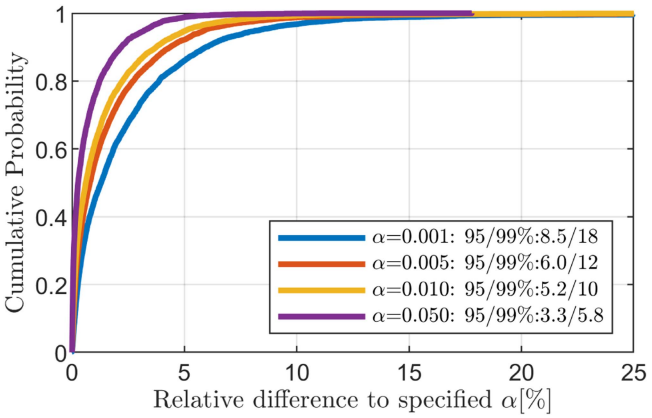

Fig. 7. Empirical CDF for relative difference of α_{LT} with respect to specified α, computed with evaluations at all locations with all model configurations. In total, 95% and 99% quantiles are provided in legend.

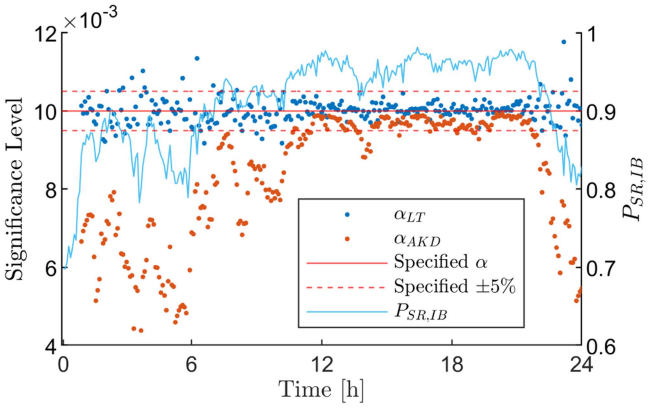

Fig. 8. Significance levels of using lookup table (α_{LT}) and AKD critical value (α_{AKD}). Experiments at location 1, with $\alpha = 1\%$ and single-frequency GPS+Galileo model for 288 epochs in 24 h.

create a lookup table in Appendix A for the users of other models or integer estimators to generate lookup tables for their own applications.

The ARD critical value is determined by the observation model and the intended significance level. To use the table and retrieve the critical value, the user needs to formulate the observation model; actual GNSS measurements are not needed for this. The lookup table saves computation effort and time compared with simulating the critical value. It also provides a significance level much closer to the specified one compared with using the AKD critical value as an approximation. The $\mathrm{ARD_{ILS}}$ can be implemented easily and efficiently with the lookup table, which can be downloaded from [1].

APPENDIX

A. PROCEDURE FOR CREATING A LOOK-UP TABLE

1) Generate many observation models by changing the number of frequencies f, constellations, observable precisions, and satellite geometries.
2) For each model, Compute the IB failure rate $1 - P_{\mathrm{SR,IB}}$ and simulate the ARD critical value κ_α.
3) Group κ_α corresponding to the same f, ambiguity-known redundancy $r(a)$, and significance level α.
4) Conduct curve fitting with each group of κ_α. Fit second-order polynomial as a function of $1 - P_{\mathrm{SR,IB}}$.
5) Save the polynomial coefficients in the lookup table with f, $r(a)$ and α as indexes.

B. PROCEDURE FOR SIMULATING SIGNIFICANCE LEVEL

1) With the given observation model, follow steps 1) to 4) described in Section III-A to generate N samples of the ARD test statistic.
2) The significance level α_{LT} corresponding to the critical value obtained with the lookup table κ_{LT} is computed as $\alpha_{LT} = N_i/N$, with N_i the number of samples larger than κ_{LT}.

REFERENCES

[1] C. Yin, "Lookup table for critical values of GNSS ambiguity-resolved detector," 4TU.ResearchData, 2024, doi: 10.4121/ca7230eb-ab5b-4554-b6ec-2d3a4f93183c.

[2] M. S. Braasch, "Multipath," in *Springer Handbook of Global Navigation Satellite Systems*. P. J.G. Teunissen and O. Montenbruck, eds., ch. 15, Cham, Switzerland: Springer, 2017, pp. 443–468.

[3] D. Lawrence, R. B. Langley, D. Kim, F.-C. Chan, and B. Pervan, "Decorrelation of troposphere across short baselines," in *Proc. IEEE/ION PLANS 2006*, 2006, pp. 94–102.

[4] L. Wanninger, "Ionospheric disturbance indices for RTK and network RTK positioning," in *Proc. 17th Int. Tech. Meeting Satell. Division Inst. Navigation (ION GNSS 2004)*, 2004, pp. 2849–2854.

[5] B. Hofmann-Wellenhof, H. Lichtenegger, and J. Collins, *Global Positioning System: Theory and Practice*. Berlin, Germany: Springer Science & Business Media, 2012.

[6] P. J.G. Teunissen, "Batch and recursive model validation," in *Springer Handbook of Global Navigation Satellite Systems*. P. J. G. Teunissen and O. Montenbruck, eds., ch. 24, pp. 687–720, Cham, Switzerland: Springer, 2017.

[7] W. Baarda, "A testing procedure for use in geodetic networks," Tech. Rep., Netherlands Geodetic Commission, vol. 2, no. 5, Delft, The Netherlands, 1968.

[8] P. J. G. Teunissen, "Testing theory: An introduction," 1st ed. Delft, The Netherlands: Delft Univ. Press, 2000.

[9] A. Leick, L. Rapoport, and D. Tatarnikov, *GPS Satellite Surveying*. Hoboken, NJ, USA: John Wiley & Sons, Inc., 2015.

[10] P. J. G. Teunissen and O. Montenbruck, *Springer Handbook of Global Navigation Satellite Systems*. Berlin, Germany: Springer, 2017.

[11] P. J. G. Teunissen, "The ambiguity-resolved detector: A detector for the mixed-integer GNSS model," *J. Geodesy*, vol. 98, no. 9, 2024, Art. no. 83.

[12] C. Yin, P. J. G. Teunissen, and C. C. J. M. Tiberius, "Performance of ambiguity-resolved detector for GNSS mixed-integer model," *GPS Solutions*, vol. 29, no. 76, 2025, Art. no. 76.

[13] P. J.G. Teunissen, "Carrier phase integer ambiguity resolution," in *Springer Handbook of Global Navigation Satellite Systems*. P. J. G. Teunissen and O. Montenbruck, eds., ch. 23, Berlin, Germany: Springer, 2017, pp. 661–685.

[14] P. J. G. Teunissen, "The probability distribution of the GPS baseline for a class of integer ambiguity estimators," *J. Geodesy*, vol. 73, pp. 275–284, 1999.

[15] P. J. G. Teunissen, "Success probability of integer GPS ambiguity rounding and bootstrapping," *J. Geodesy*, vol. 72, pp. 606–612, 1998.

[16] P. J. G. Teunissen, "An optimality property of the integer least-squares estimator," *J. Geodesy*, vol. 73, pp. 587–593, 1999.

[17] C. Yin, P. J. G. Teunissen, and C. C. J. M. Tiberius, "Implementation of ambiguity-resolved detector for high-precision GNSS fault detection," in *Proc. 37th Int. Tech. Meeting Satell. Division Inst. Navigation (ION GNSS 2024)*, 2024, pp. 2163–2174.

[18] A. Wieser, "Reliability checking for GNSS baseline and network processing," *GPS Solutions*, vol. 8, pp. 55–66, 2004.

[19] A. El-Mowafy, "GNSS multi-frequency receiver single-satellite measurement validation method," *GPS Solutions*, vol. 18, pp. 553–561, 2014.

[20] S. Hewitson and J. Wang, "GNSS receiver autonomous integrity monitoring (RAIM) performance analysis," *GPS Solutions*, vol. 10, pp. 155–170, 2006.

[21] J. K. Lee, J. O. Lee, and J. O. Kim, "New quality control algorithm based on GNSS sensing data for a bridge health monitoring system," *Sensors*, vol. 16, no. 6, 2016, Art. no. 774.

[22] B. Li, L. Zhang, and S. Verhagen, "Impacts of Beidou stochastic model on reliability: Overall test, w-test and minimal detectable bias," *GPS Solutions*, vol. 21, pp. 1095–1112, 2017.

[23] P. J. G. Teunissen, "The least-squares ambiguity decorrelation adjustment: A method for fast GPS integer ambiguity estimation," *J. Geodesy*, vol. 70, pp. 65–82, 1995.

[24] S. Verhagen, B. Li, and P. J. G. Teunissen, "Ps-LAMBDA: Ambiguity success rate evaluation software for interferometric applications," *Comput. Geosciences*, vol. 54, pp. 361–376, 2013.

[25] L. Massarweh, S. Verhagen, and P. J. G. Teunissen, "New LAMBDA toolbox for mixed-integer models: Estimation and evaluation," *GPS Solutions*, vol. 29, no. 14, 2025, Art. no. 14.

[26] S. Verhagen, "On the approximation of the integer least-squares success rate: Which lower or upper bound to use," *J. Glob. Positioning Syst.*, vol. 2, no. 2, pp. 117–124, 2003.

[27] P. J. G. Teunissen, "The parameter distributions of the integer GPS model," *J. Geodesy*, vol. 76, pp. 41–48, 2002.

[28] P. J. G. Teunissen and A. Khodabandeh, "Review and principles of PPP-RTK methods," *J. Geodesy*, vol. 89, no. 3, pp. 217–240, 2015.

[29] D. Odijk, B. Zhang, A. Khodabandeh, R. Odolinski, and P. J. G. Teunissen, "On the estimability of parameters in undifferenced, uncombined GNSS network and PPP-RTK user models by means of S-system theory," *J. Geodesy*, vol. 90, no. 1, pp. 15–44, 2016.

[30] H.-J. Eueler and C. C. Goad, "On optimal filtering of GPS dual frequency observations without using orbit information," *Bull. Géodésique*, vol. 65, pp. 130–143, 1991.

[31] R. J. Serfling, *Approximation Theorems of Mathematical Statistics*. Hoboken, NJ, USA: Wiley, 1980.

[32] P. Bona, "Precision, cross correlation, and time correlation of GPS phase and code observations," *GPS Solutions*, vol. 4, no. 2, pp. 3–13, 2000.

[33] A. Amiri-Simkooei, F. Zangeneh-Nejad, and J. Asgari, "Least-squares variance component estimation applied to GPS geometry-based observation model," *J. Surveying Eng.*, vol. 139, no. 4, pp. 176–187, 2013.

[34] P. Hou, B. Zhang, and Y. Yuan, "Analysis of the stochastic characteristics of GPS/BDS/Galileo multi-frequency observables with different types of receivers," *J. Spatial Sci.*, vol. 66, no. 1, pp. 49–73, 2021.

[35] G. Johnston, A. Riddell, and G. Hausler, "The international GNSS service," in *Springer Handbook Glob. Navigation Satell. Syst.*, Cham, Switzerland: Springer, 2017, pp. 967–982.

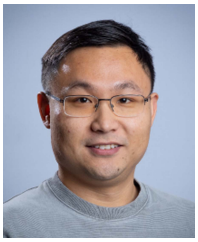

Chengyu Yin received the bachelor's degree in navigation engineering from Wuhan University, Wuhan, China, in 2018, and the master's degree in earth-oriented space science and technology from the Technical University of Munich, Munich, Germany, in 2021.

He is a Ph.D. candidate with the Delft University of Technology, Delft, The Netherlands. His current research interests include carrier phase ambiguity resolution and quality control theory for high-precision GNSS positioning.

Peter J.G. Teunissen received the Ph.D. degree in mathematical geodesy from the Delft University of Technology, Delft, The Netherlands, in 1985. He is a Professor of geodesy and satellite navigation with the Delft University of Technology, and a Member of the Royal Netherlands Academy of Arts and Sciences. His past academic positions include the Head of the Delft Earth Observation Institute, Science Director of the Australian Centre for Spatial Information and Federation Fellow of the Australian Research Council. He has been research-active in various fields of Earth Observation, with current research focused on the development of theory, models, and algorithms for high-accuracy applications of satellite navigation and remote sensing systems.

Christian C.J.M. Tiberius received the Ph.D. degree in recursive data processing for kinematic GPS surveying from the Delft University of Technology, Delft, The Netherlands, in 1998.

He is currently an Associate Professor with the Geoscience and Remote Sensing Department, Delft University of Technology. His research interests include navigation, with GNSS and terrestrial radio positioning, primarily for automotive applications.